

# Three particles in an external trap: Nature of the complete $J = 0$ spectrum

D. Blume<sup>(1)</sup> and Chris H. Greene<sup>(2)</sup>

<sup>(1)</sup>*Department of Physics, Washington State University, Pullman, WA 99164-2814, USA;*

<sup>(2)</sup>*Department of Physics and JILA, University of Colorado, Boulder, CO 80309-0440, USA*

(November 1, 2018)

Three bosonic, spin-polarized atoms in a spherical oscillator potential constitutes the simplest nontrivial Bose-Einstein condensate (BEC). The present paper develops the tools needed to understand the nature of the complete  $J = 0$  energy spectrum for this prototype system, assuming a sum of two-body potentials. The resulting spectrum is calculated as a function of the two-body scattering length  $a_{sc}$ , which documents the evolution of certain many-body levels that evolve from BEC-type to molecular-type as the scattering length is decreased. Implications for the behavior of the condensate excited-state spectrum and for condensate formation and decay are elucidated. The energy levels evolve smoothly, even through the regime where the number of two-body bound states  $N_b$  increases by 1, and  $a_{sc}$  switches from  $-\infty$  to  $+\infty$ . We point out the possibility of suppressing three-body recombination by tuning the two-body scattering length to values that are larger than the size of the condensate ground state. Comparisons with mean-field treatments are presented.

## I. INTRODUCTION

Mean-field methods are commonly used to characterize Bose-Einstein condensates (BECs), i.e., atomic alkali vapors in an external trapping potential [1]. These approaches, which account for the interaction between particles through a mean-field term in an effective single-particle Hamiltonian, accurately describe much of the dilute condensate energetics. However, these shape-independent  $s$ -wave scattering length approximations break down for strongly interacting gases with large interaction parameters [1–5].

Very recent experiments by Greiner *et al.* [6,7] have entered this regime: A quantum phase transition from a superfluid to a Mott insulator was observed for ultracold atoms held in a three-dimensional optical lattice. Most relevant to our studies here, the atoms are held in tight *isotropic* lattice sites with an occupancy of 1-3 atoms per site. The experiment thus realizes a strongly correlated many-body (and in a sense, few-body) quantum system with unprecedented control of parameters. In this paper, we present the quantal  $J = 0$  energy spectrum of three particles under external isotropic confinement, and compare with results obtained using mean-field theory.

The lowest order mean-field approximation [Gross-Pitaevskii (GP) or Hartree-Fock (HF) equation] [1,8–11] and also higher order approaches such as second order perturbation theory [12,13] treat the metastable BEC state of the trapped alkali vapor as if it was the “true” ground state of the system. This means that these approaches cannot describe recombination processes or atom-loss processes, since coupling to the true (solid-like/liquid-like) ground state is neglected completely. Attempts to include additional “empirical” terms in these mean-field equations, which account for “reaction processes”, exist, and have been able to describe some experimental findings successfully [14–16]. However, the ad hoc nature of some of these empirical terms is less than satisfactory.

The nonperturbative quantal calculations permit us to circumvent these problems. These calculations come at a price, namely, our initial restriction to only  $N = 3$  particles with total angular momentum  $J = 0$  in the trap. For this “simple” system, however, we are able to include all channels in the calculation, molecular three-body bound state channels, diatom plus atom channels, and metastable gaseous-like channels [17].

This paper focuses on regimes where standard mean-field treatments break down. For large positive  $a_{sc} \rightarrow +\infty$ , the mean-field treatment results in unphysically large diverging energies. In contrast, the three-body energies change smoothly in the pole region, where the scattering length  $a_{sc}$  changes from  $-\infty$  to  $+\infty$  and the number of two-body  $s$ -wave bound states  $N_b$  increases by 1. Additionally, our three-body study implies that the excitation frequencies are well behaved around  $|a_{sc}| \rightarrow \infty$ .

The mean-field treatment also exhibits limitations in the parameter range around the negative critical scattering length  $a_{cr}$ , where  $a_{cr}$  is defined through the instability criterion  $(N - 1)a_{cr}/a_{ho} = -0.575$  derived from the mean-field equation [11,18]. The lowest gaseous energy level (i.e., the BEC ground state) changes its character from metastable to molecular around  $a_{cr}$ , while some of the higher lying BEC-like states remain almost completely unaffected by criticality. In contrast, the mean-field equation simply has no solution for  $a_{sc}$  lower than the critical value.

Three-particle studies have been used previously to shed light on the many-body physics of BECs. In 1996, Esry *et al.* [19] explored the role of the two-body scattering length in BECs. More recently, three research groups explained experiments regarding the three-body recombination rate in many-atom BECs via three-body calculations that include channel coupling [17,20–23]. Three-body studies have also been used to test the validity of shape-independent two-body interaction potentials [24].

The studies presented here are based on time-independent Schrödinger wave mechanics. The energy levels show several avoided crossings when plotted as functions of  $a_{sc}$  (see Section III); nevertheless, dynamical behavior such as Landau-Zener-type branching ratios or recombination rates remains beyond the scope of this paper. Studies along these lines will be a natural continuation of the static studies presented here.

Section II describes our three-body system, and outlines the formalism for its investigation. Section III presents quantum mechanical three-body energetics, and Section IV compares with results derived from mean-field treatments. Finally, Section V summarizes our main results.

## II. THE THREE-PARTICLE SYSTEM

The Schrödinger equation for three mass- $m$  particles in a spherical external potential with trapping frequency  $\nu_{ho} = \omega_{ho}/(2\pi)$  reads

$$\left[ \sum_{i=1}^3 -\frac{\hbar^2}{2m} \nabla_{\vec{r}_i}^2 + \sum_{i=1}^3 \frac{1}{2} m \omega_{ho}^2 r_i^2 + \sum_{i<j}^3 V(r_{ij}) \right] \Psi(\vec{r}_1, \vec{r}_2, \vec{r}_3) = E \Psi(\vec{r}_1, \vec{r}_2, \vec{r}_3), \quad (1)$$

where  $V(r_{ij})$  denotes a two-body interaction potential and  $r_{ij} = |\vec{r}_j - \vec{r}_i|$ .  $\vec{r}_i$  is the position vector of atom  $i$  relative to the center of the trap. Restriction to states of zero total angular momentum ( $J = 0$ ) reduces this nine-dimensional problem to six dimensions. The dimensionality of the problem can be reduced further by a transformation to Jacobi coordinates,  $\vec{X}_{cm} = (\vec{r}_1 + \vec{r}_2 + \vec{r}_3)/3$ ,  $\vec{\rho}_{12} = \vec{r}_2 - \vec{r}_1$ , and  $\vec{\rho}_{12,3} = \vec{r}_3 - (\vec{r}_2 + \vec{r}_1)/2$  [24]. This transformation decouples the center-of-mass motion,

$$\left( -\frac{\hbar^2}{2M} \nabla_{\vec{X}}^2 + \frac{1}{2} M \omega_{ho}^2 X^2 \right) \phi_{klm}(\vec{X}) = E_k^{CM} \phi_{klm}(\vec{X}), \quad (2)$$

from the relative (internal) motion,

$$\left[ -\frac{\hbar^2}{2\mu} \frac{\partial^2}{\partial R^2} + \frac{1}{2} \mu \omega_{ho}^2 R^2 + \frac{\hbar^2}{2\mu R^2} \left( \Lambda^2 + \frac{15}{4} \right) + \sum_{i<j}^3 V(r_{ij}) \right] \psi_n(R, \vartheta, \varphi) = E_n^{int} \psi_n(R, \vartheta, \varphi). \quad (3)$$

Here,  $M = 3m$  is the total mass, and  $E_k = (k + 3/2)\hbar\omega_{ho}$  with  $k = 0, 1, 2, \dots$  the energy related to the center-of-mass motion. The corresponding eigenfunctions  $\phi_{klm}$  are simply the three-dimensional isotropic oscillator solutions. Eq. (3) represents the Hamiltonian describing the relative particle motions in terms of three hyperspherical coordinates ( $R, \vartheta, \varphi$ ) rather than the Jacobi coordinates  $\vec{\rho}_{12}$  and  $\vec{\rho}_{12,3}$  [24–27]. Our definition of the hyperradius  $R$ , and the two hyperangles  $\vartheta$  and  $\varphi$  is based on the democratic coordinate system of Whitten-Smith [28], i.e.,  $\mu R^2 = m\rho_{12}^2/2 + 2m\rho_{12,3}^2/3$ . Owing to the identical boson character of the atoms, the angular range can be restricted to  $\varphi \in [0, \pi/6]$  and  $\vartheta \in [0, \pi/4]$ .  $\mu = m/\sqrt{3}$  denotes the reduced mass of the three-body system, while  $\Lambda^2$  denotes the “squared grand angular momentum” operator [29]. Here we rescale the wave function  $\psi(R, \vartheta, \varphi)$  by  $R^{5/2}$ , i.e.  $\Psi(\vec{r}_1, \vec{r}_2, \vec{r}_3) = R^{-5/2} \psi(R, \vartheta, \varphi) \phi_{klm}(\vec{X})$ , in order to eliminate first derivatives from the hyperradial kinetic energy operator.

Eq. (3) is solved here using two different, but related approaches: a coupled-adiabatic-channels approach and a strict adiabatic approximation. The coupled-adiabatic-channel calculation can in principle be made exact. The strict adiabatic approximation can be viewed as an “incomplete” coupled-adiabatic-channel calculation, truncated to one channel only, which neglects all off-diagonal coupling elements. It is important to keep in mind that the strict adiabatic approximation cannot describe recombination processes.

To solve Eq. (3) we expand  $\psi_n(R, \vartheta, \varphi)$  into radial wave functions  $F_{\nu n}(R)$  and a set of complete, orthonormal angular channel functions  $\Phi_{\nu}(R; \vartheta, \varphi)$ . The basis functions  $\Phi_{\nu}$ , which depend parametrically on  $R$ , are solutions of the partial differential equation

$$\left[ \frac{\hbar^2}{2\mu R^2} \left( \Lambda^2 + \frac{15}{4} \right) + \sum_{i<j}^3 V(r_{ij}) \right] \Phi_{\nu}(R; \vartheta, \varphi) = U_{\nu}(R) \Phi_{\nu}(R; \vartheta, \varphi). \quad (4)$$

We refer to the eigenvalues  $U_\nu(R)$  as adiabatic potential curves. Inserting the expansion  $\psi_n = \sum F_{\nu n} \Phi_\nu$  into the Schrödinger equation for the internal motion [Eq. (3)] results in an infinite set of coupled ordinary differential equations,

$$\left( -\frac{\hbar^2}{2\mu} \frac{d^2}{dR^2} + \frac{1}{2} \mu \omega_{ho}^2 R^2 + U_\nu(R) + Q_{\nu\nu}(R) - E_n^{int} \right) F_{\nu n}(R) = - \sum_{\nu' \neq \nu} Q_{\nu\nu'}(R) F_{\nu' n}(R) + \sum_{\nu' \neq \nu} P_{\nu\nu'}(R) \frac{dF_{\nu' n}(R)}{dR}, \quad (5)$$

where  $P_{\nu\nu'}$  [ $Q_{\nu\nu'}$ ] are angular coupling matrix elements involving the first [second] derivative of  $\Phi_\nu$  with respect to  $R$  [30]. We refer to the solution of Eq. (5) as the coupled-adiabatic-channel solution. The strict adiabatic approximation follows immediately by neglecting coupling elements between different channels [ $\equiv$  setting the right hand side of Eq. (5) to zero]. Another variant of the strict adiabatic approximation additionally neglects the diagonal element  $Q_{\nu\nu}$ , and is typically referred to as the hyperspherical Born-Oppenheimer approximation. In the following, we use these two variants of the strict adiabatic approximation interchangeably, and denote the eigenvalues by  $E_{\nu n}^{int}$ .

The outlined formalism splits the solution of the Schrödinger equation for the internal motion [Eq. (3)] into two steps: *i*) solution of Eq. (4) (here via a two-dimensional B-spline code), and *ii*) solution of the one-dimensional coupled equations, Eq. (5). The former is numerically more challenging due to its higher dimensionality, and coincides with determining the bound and continuum channel functions  $\Phi_\nu$  of three particles interacting via a sum of two-body potentials  $V(r)$  [the trapping potential does not enter Eq. (4)].

For a vanishing interaction potential,  $V(r) = 0$ , the eigenfunctions  $\Phi_\nu$  of Eq. (4) reduce to Gegenbauer polynomials [29] with eigenvalues  $U_\nu(R) = \hbar^2 \frac{\lambda(\lambda+1)+15/4}{2\mu R^2}$ ,  $\lambda = 0, 4, 6, \dots$ , where the  $\lambda = 2$  state is forbidden due to symmetry constraints, and the eigenvalues with  $\lambda = 12$  and  $\lambda \geq 16$  are doubly-degenerate. Now consider a non-vanishing two-body interaction potential  $V(r)$ . Compared to the  $V = 0$  potential, the non-vanishing  $V$  introduces three-body bound states at small hyperradii  $R$ , accounting for the short range physics of  $V(r)$ , and also modifies the potential curves at large  $R$ , reflecting the non-zero  $s$ -wave scattering length  $a_{sc}$ . Additionally, a non-vanishing  $V$  lifts the degeneracy of the  $U_\nu(R)$  potential curves.

To illustrate this behavior, Fig. 1 shows the sum of the trapping potential,  $V_{trap} = \mu\omega_{ho}^2 R^2/2$  with  $\nu_{ho} = 78\text{kHz}$ , and the adiabatic potential curves,  $U_\nu(R)$ , for a two-body model interaction potential (see Sec. III) with  $s$ -wave scattering length  $a_{sc} = 228a.u.$  and two two-body  $s$ -wave bound states,  $N_b = 2$  [ $m = m(^{87}\text{Rb})$ ]. Length and energy are expressed in oscillator units (length unit  $a_{ho} = \sqrt{\hbar/(m\omega_{ho})}$ , energy unit  $\hbar\omega_{ho}$ ). The two lowest potential curves with  $\nu = 0$  and 1 (upper panel, dashed lines) describe three-body bound state physics, and approach the two-body  $s$ -wave binding energies in the absence of a trapping potential. The higher lying potential curves (solid lines) describe metastable BEC physics, and would correspond to continuum states, in the absence of a trapping potential. The  $\nu = 2$  curve (thick solid line) shows a double minimum structure with minima at  $R \approx 0.2a_{ho}$  and  $R \approx 2.5a_{ho}$ , which are separated by a potential barrier. The lowest metastable state “lives” in the minimum at larger  $R$ . The lower panel of Fig. 1 shows an enlargement of the gaseous region together with the effective potential curves for a vanishing interaction potential (dotted lines). Significant deviations between the solid and the dotted curves (non-vanishing and vanishing two-body potential, respectively) are visible.

As clearly demonstrated in Fig. 1, to properly describe the metastable states, one must solve Eq. (4) for hyperradii  $R$  as large as  $10a_{ho}$ , corresponding roughly to several  $10^4 a.u.$  (depending somewhat on  $\nu_{ho}$ ). In our calculation, we determine the adiabatic potential curves  $U_\nu$  and the coupling matrix elements  $P_{\nu\nu'}$  and  $Q_{\nu\nu'}$  out to  $R \approx 10 - 100a_{sc}$  using a two-dimensional B-spline code, and then extrapolate to larger  $R$ . For the continuum potential curves we follow a second independent approach suggested by Nielsen and Macek [20]. For large  $R$ , they recognise the dependence of  $U_\nu$  on  $a_{sc}$  only, and derive a nearly analytic expression for  $U_\nu$ . Note, Nielsen and Macek’s formula does not account for those potential curves, which simply coincide with the “unperturbed” eigenvalues  $\hbar^2 \frac{\lambda(\lambda+1)+15/4}{2\mu R^2}$ ,  $\lambda = 12, 16, 18, \dots$  (see above). The nearly analytical expressions [20] are in excellent agreement with our continuum curves  $U_\nu$  calculated through numerical solution (and extrapolation) of Eq. (4).

In passing, we note an additional nice feature of the outlined formalism. Suppose that we wish to study the energetics of three particles in an external spherical potential as a function of the trapping frequency  $\nu_{ho}$ . For a given interaction potential  $V(r)$ , it is only necessary to solve the numerically most demanding Eq. (4) once.  $\omega_{ho}$  then enters the simple one-dimensional Eq. (5) simply through an additive term, which trivially determines the energy spectrum versus  $\omega_{ho}$ .

### III. THE QUANTAL ENERGY SPECTRUM

This section presents the internal energies  $E^{int}$  for three bosonic particles with  $J = 0$  in an external trap for a two-body model potential of the form  $V(r) = d \cosh^{-2}(r/r_0)$ . This is convenient because the two-body  $s$ -wave eigenenergies and eigenfunctions can be determined analytically [31]. Furthermore, we determined an analytical expression for the energy-dependent  $s$ -wave scattering length,

$$a_{sc}(k) = \frac{1}{ik} \frac{1 + \rho}{1 - \rho}, \quad (6)$$

where

$$\rho = -\frac{{}_2F_1(ik - s, 1 + s + ik; 1 + ik; \frac{1}{2})}{2^{ik} {}_2F_1(-s, 1 + s; 1 - ik; \frac{1}{2})}, \quad (7)$$

where  $k = \sqrt{mE/\hbar^2}$ , and  $s = -\frac{1}{2} + \frac{1}{2}\sqrt{1 + 4mdr_0^2/\hbar^2}$ .  ${}_2F_1$  denotes the usual hypergeometric function. The zero-energy  $s$ -wave scattering length  $a_{sc}$  is then simply given by  $a_{sc} = \lim_{k \rightarrow 0} a_{sc}(k)$ . While  $r_0$  is fixed at  $r_0 = 55a.u.$  throughout our calculations,  $d$  is varied to change the number of two-body  $s$ -wave bound states  $N_b$  and the two-body  $s$ -wave scattering length  $a_{sc}$  [ $m = m(^{87}\text{Rb})$  throughout the rest of the paper]. We perform three-body calculations for 70 different  $d$  values, which translates into a range of two-body scattering lengths  $a_{sc}$  from  $-10^4 a.u.$  to  $10^4 a.u.$ . To keep the coupled-adiabatic-channel calculations tractable we restrict  $d$  in this study to values such that  $N_b = 1$  or 2.

Consider a vanishing interaction potential,  $d = 0$  (ideal gas) first. For this system, the strict adiabatic approximation is exact, and  $E_n^{int} = 3, 5, 7, \dots \hbar\omega_{ho}$ . Introduction of a non-vanishing interaction potential shifts these gaseous energy levels according roughly to the value of  $a_{sc}$ , lifts the degeneracy, and additionally gives rise to three-body bound states. Figure 2 shows the internal energies  $E_{\nu n}^{int}$  (solid lines) of the gaseous-like states for  $\nu_{ho} = 78\text{kHz}$  calculated via the strict adiabatic approximation for various scattering lengths  $a_{sc}$ . To accommodate a large range of interaction parameters  $(N-1)a_{sc}/a_{ho}$  [11], Fig. 2 shows the internal energies as a function of  $[\arctan(a_{sc}/a_{ho})]/\pi$ . To additionally be able to plot results for systems with  $N_b = 1$  and  $N_b = 2$  two-body bound states, respectively, the integer part of the abscissa is chosen to be equal to  $-N_b$ . This scaling procedure results in abscissa values of  $[-2.5, -0.5]$ . We refer to the interval  $[-0.5, -1.5]$  as the “first cycle” ( $N_b = 1$ ), and to the interval  $[-1.5, -2.5]$  as the “second cycle” ( $N_b = 2$ ). In this representation,  $a_{sc} = 0$  corresponds to  $[\arctan(a_{sc}/a_{ho})]/\pi = -2.0$  and  $-1.0$ .

To interpret this complicated energy level structure, concentrate on six different scattering length values labeled by A–F in Fig. 2. Figure 3 shows the sum of the corresponding adiabatic potential curves and the trapping potential,  $U_\nu + V_{trap}$ , where  $V_{trap}(R) = 0.5\mu\omega_{ho}^2 R^2$  (solid lines):

Panel A corresponds to a large positive scattering length,  $a_{sc} = 2138a.u.$ . The lowest BEC-like curve ( $\nu = 2$ ) is highlighted as a thick solid curve. The lowest energy level lying within this potential curve,  $E_{20}^{int}$ , has an energy close to  $5\hbar\omega_{ho}$ , and the excited levels ( $E_{2n}^{int}$ ,  $n > 0$ ) lie about  $2\hbar\omega_{ho}$  higher each (see Fig. 2). We refer to the energy levels “located” within the same potential curve (identical  $\nu$ , but having a different number of hyperradial nodes  $n$ ) as a family. The lowest energy of the next higher BEC-like curve is  $E_{30}^{int} \approx 7\hbar\omega$ , and again, the excited levels ( $E_{3n}^{int}$ ,  $n > 0$ ) lie about  $2\hbar\omega_{ho}$  higher each. To guide the eye, Fig. 2 displays dotted curves that represent the effective potential curves in the absence of any two-body interaction potential.

Panel B corresponds to a much smaller scattering length than in panel A,  $a_{sc} = 103a.u.$ . This panel shows a series of crossings at energies around  $20\hbar\omega_{ho}$ , indicating a  $d$ -wave shape resonance. As the scattering length decreases slightly, these crossings move to lower energies, until they finally vanish at  $a_{sc} = 97a.u.$ . The scattering length  $a_{sc} = 97a.u.$  corresponds to a well depth  $d$  of the two-body potential  $V$  at which  $V$  first supports a  $d$ -wave two-body bound state. To calculate energy levels in the presence of a  $d$ -wave shape resonance we follow the potential curves that cross diabatically. Note that the potential curves approach the  $V(r_{ij}) = 0$  curves (i.e., the dotted lines) as  $a_{sc}$  approaches zero. Accordingly, the energy levels approach those of the ideal inhomogeneous gas.

Panel C shows the effective potential curves (solid lines) for vanishing scattering length,  $a_{sc} = 0$  (however, non-vanishing  $V$ ), in which case the potential curves are almost identical to the ones for vanishing  $V$  (dotted lines). Small differences occur in the inner wall region reflecting the existence of molecular states at small  $R$ . These molecular states at small  $R$  are, however, not shown in Fig. 3.

Panels D, E, and F correspond to negative scattering lengths. The inflection of the thick solid line at  $R \approx 0.5a_{ho}$  in panel D indicates the first signature of a decaying condensate. The interaction parameter for this system is  $(N-1)a_{sc}/a_{ho} = -0.085$ . In panel E, the barrier of the lowest gaseous-like curve, which separates the BEC minimum from the energetically much deeper molecular minimum, has almost vanished; here,  $(N-1)a_{sc}/a_{ho} = -0.356$ . Panel F shows a large negative scattering length case,  $a_{sc} = -1970a.u.$ . The thick solid curve corresponds to a situation

in which the gaseous-like state (condensate) is no longer stable. Note the similarity of the potential curves for large positive and large negative  $a_{sc}$  (panel A and F). This similarity reflects the smooth dependence of  $E_{\nu_n}^{int}$  as  $|a_{sc}|$  goes through infinity (see below).

In addition to the aforementioned issues, four more characteristics are important to the energy level scheme shown in Fig. 2: (i) At  $a_{sc} = 0$ , corresponding to  $[\arctan(a_{sc}/a_{ho})]/\pi = -1$  and  $-2$ , the positive energy levels  $E_{\nu_n}^{int}$  lie very close to those of the ideal gas. (ii) The energy level with energy  $E^{int} = 15\hbar\omega_{ho}$  is unchanged over the two cycles shown. This energy level originates in the “unperturbed” potential curve  $\hbar^2 \frac{\lambda(\lambda+1)+15/4}{2\mu R^2}$ ,  $\lambda = 12$  (see Section II), and therefore coincides with an ideal gas level. (iii) The internal energy levels in the first cycle ( $N_b = 1$ ) and in the second cycle ( $N_b = 2$ ) behave very similarly, indicating that the energies are, to a good approximation, independent of the number of two-body  $s$ -wave bound states  $N_b$ . (iv) Notice in particular that the energy levels  $E_{\nu_n}^{int}$  change smoothly as  $|a_{sc}|$  passes through infinity.

Note as well that families of plunging energy levels with molecular character are present, which to simplify our presentation are shown only partially in Fig. 2. Consider the lowest gaseous-like energy level of the first cycle, i.e. with  $N_b = 1$ . As the gaseous-like state becomes unstable while  $a_{sc}$  decreases this energy level decreases through zero (at  $[\arctan(a_{sc}/a_{ho})]/\pi \approx -1.2$ ), which reflects the transition of this BEC state to one of molecular character. The other energy levels of this family also change character from gaseous-like to molecular-like as the two-body potential well depth  $d$  becomes deeper. For clarity, Fig. 2 shows these energy levels only for  $[\arctan(a_{sc}/a_{ho})]/\pi > -1.75$ . For each additional two-body bound state, a “manifold” of plunging energy levels is present, reflecting the fact that the number of three-body states with negative energy increases far more rapidly than those for the two-body system.

So far we have discussed results for a trap with trapping frequency  $\nu_{ho} = 78\text{kHz}$ . In addition, we performed calculations for trapping frequencies that are 10 times larger, and also 10 or 100 times smaller. Since  $a_{ho} = \sqrt{\hbar/(m\omega_{ho})}$ , the interaction parameter  $(N - 1)a_{sc}/a_{ho}$  scales as  $\sqrt{\omega_{ho}}$ . Adopting the same two-body interaction potentials as before, a trapping frequency smaller than  $\nu_{ho} = 78\text{kHz}$  therefore leads to a narrower  $[\arctan(a_{sc}/a_{ho})]/\pi$  interval than shown in Fig. 2. As an example, Fig. 4 shows the internal energies  $E_{\nu_n}^{int}$  for three particles in a trap with  $\nu_{ho} = 780\text{Hz}$  and  $N_b = 2$  (solid lines). A few of the internal energies at large negative scattering length, corresponding to  $[\arctan(a_{sc}/a_{ho})]/\pi \approx -2.08$ , are indicated by diamonds. These data points are not connected by solid lines since in this region our grid in  $a_{sc}$  is too coarse to allow for interpolation.

To summarize, our microscopic studies of the energetics of three confined particles as a function of  $\nu_{ho}$  reveal that the overall behavior of the energy level scheme (as shown in Fig. 2) remains unchanged as  $\nu_{ho}$  either decreases or increases. As discussed in the previous paragraph, however,  $\nu_{ho}$  determines the range of the interaction parameter. Specifically, the behavior of the energy levels around  $a_{sc} \approx a_{cr}$  depends on  $\nu_{ho}$ . Figure 2 indicates a gradual decrease of the condensate energy as the scattering length decreases through the region  $[\arctan(a_{sc}/a_{ho})]/\pi \approx -2.1$ . As  $\nu_{ho}$  is decreased, the separation between the molecular-like region at small  $R$  and the gaseous-like region at large  $R$  becomes more pronounced, and the energy decrease (change from gaseous-like to molecular-like) takes place over a smaller range of scattering lengths. In other words, the potential barrier (shown in panel D and E of Fig. 3 for  $\nu_{ho} = 78\text{kHz}$ ) spatially separates the molecular-like and gaseous-like region more for small  $\nu_{ho}$  than for large  $\nu_{ho}$ .

The internal energies discussed in this section have been calculated within the strict adiabatic approximation. To assess the accuracy of this approach we additionally performed coupled-adiabatic-channel calculations. Figure 5 shows the energies resulting from the coupled-adiabatic-channel calculation including four channels (pluses) together with those resulting from the adiabatic calculation (dotted, solid, and dashed lines) for  $\nu_{ho} = 78\text{kHz}$ . Figure 5 indicates excellent agreement between these two sets of calculations for small  $a_{sc}$  (left hand side of the figure), however, some differences occur at larger  $a_{sc}$  (right hand side of the figure). To be more specific, the plunging molecular levels (dotted lines) and the BEC levels in the lowest gaseous adiabatic potential curve (solid lines) seem to repel each other at large  $a_{sc}$  due to channel coupling. In summary, for our time-independent studies here, the strict adiabatic approximation describes the main characteristics of the energy level pattern as shown in Figs. 2 and 4 with sufficient accuracy. To go beyond this static picture, however, the coupling between channels must be considered.

Studies including channel coupling [17,19] show that the primary recombination mechanism is related to the behavior of the adiabatic potential curves and the corresponding coupling elements at hyperradii  $R \approx 2 - 3a_{sc}$ . Consider panel A of Fig. 3 with  $a_{sc} = 2138\text{a.u.}$  and  $\nu_{ho} = 78\text{kHz}$ . For this situation, the criterion  $R \approx 2 - 3a_{sc}$  translates into  $5.8 - 8.8a_{ho}$ . At these hyperradii, the lowest lying gaseous  $V_{trap} + U_\nu$  curve reaches  $\approx 10 - 20\hbar\omega_{ho}$ , compared to the lowest gaseous energy level of  $\approx 5.3\hbar\omega_{ho}$ . Thus, we speculate that we have entered a regime where recombination processes are largely suppressed due to the strong confinement. It would be interesting to probe this regime experimentally.

#### IV. COMPARISON WITH MEAN-FIELD TREATMENTS

This section connects our microscopic studies with results obtained by mean-field treatments. Consider the HF treatment [11], which results in an equation identical to the GP equation, except for a change from  $N$  to  $N - 1$  in the interaction parameter. The HF treatment does not take advantage of the decoupling of the center-of-mass and the internal motion, and determines an approximate value for the total energy  $E_{HF}$  as well as the orbital energy or chemical potential. To compare our internal three-body energies  $E_{\nu n}^{int}$  (solid lines in Figs. 2 and 4) with the HF energy  $E_{HF}$ , we subtract the exact energy associated with the lowest center-of-mass motion,  $E_0^{CM} = 1.5\hbar\omega_{ho}$ , from  $E_{HF}$ , and refer to this quantity as internal HF energy  $E_{HF}^{int}$ . The approximate HF treatment could either lead to an error in  $E_{HF}^{int}$  or in  $E_{HF}^{CM}$ , or in both these quantities at the same time, and the subtraction of  $E_0^{CM}$  from  $E_{HF}$  is therefore somewhat artificial [32]. Figures 2 and 4 show the resulting internal HF energy,  $E_{HF}^{int}$ , as dotted lines.

For  $\nu_{ho} = 780\text{Hz}$ , the internal HF energy  $E_{HF}^{int}$  (dotted lines in Fig. 4) agrees favorably with the lowest gaseous-like internal three-body energy (solid line). As discussed in Sec. III, Fig. 4 includes only a small range of interaction parameters  $(N - 1)a_{sc}/a_{ho}$ . Thus, the good agreement between  $E_{\nu n}^{int}$  and  $E_{HF}^{int}$  is not surprising.

For comparison, Fig. 2 shows the energy levels for a 100 times larger trapping frequency, namely  $\nu_{ho} = 78\text{kHz}$ . This figure indicates two regions in which  $E_{HF}^{int}$  (dotted line) deviates from the lowest many-body energy level  $E_{\nu n}^{int}$  having gaseous character, the region around  $a_{cr}$  and the large  $a_{sc}$  region. For  $a_{sc} \leq a_{cr}$ , the HF equation does not have a solution. This mathematical fact is typically interpreted as “decay of the condensate” [1,18]. The three-body treatment reveals that the decay of the condensate is linked to the disappearance of a potential barrier (see, e.g., panels D and E of Fig. 3), which separates the molecular region at small  $R$  from the gaseous-like region at large  $R$ . When the potential barrier has disappeared, the states associated with this potential curve have purely molecular character. Thus, the energy levels in this potential curve change dramatically in the vicinity of  $a_{cr}$ , whereas most of the energy levels belonging to other families change slowly around  $a_{sc}$ .

Our interpretation of the behavior of a BEC in the vicinity of  $a_{cr}$  agrees with that suggested by Bohn *et al.* for an arbitrary number of particles [33]. Within the  $K$ -harmonic approximation, Bohn *et al.* [33] describe the interaction between each pair of particles through a shape-independent delta-function potential, and make some approximations about the behavior at small hyperradii, where the  $\delta$ -function potential leads to divergences. These approximations are confirmed to be well justified, based on our calculations with shape-dependent two-body interaction potentials, so that no additional approximations at small  $R$  need to be made. Taken together, these two studies highlight the usefulness of the hyperspherical radius coordinate in interpreting dynamics of a BEC (see also [34]).

Figure 2 also indicates discrepancies between  $E_{HF}^{int}$  and  $E_{\nu n}^{int}$  at large  $|a_{sc}|$ . For  $a_{sc} \rightarrow \infty$ ,  $E_{HF}^{int}$  diverges and approaches unrealistically large values, whereas the three-body energies  $E_{\nu n}^{int}$  behave smoothly. Recall that the sign change of the scattering length from  $-\infty$  to  $+\infty$  (pole region) corresponds to the appearance of an additional two-body  $s$ -wave bound state. Coincidentally, this corresponds to the existence of a hyperradial potential curve, which approaches the corresponding (negative) two-body binding energy in the absence of the trapping potential asymptotically. Around the pole region, this hyperradial potential curve is energetically close to the lowest potential curve with gaseous-like character, and therefore, coupling between these two potential curves with molecular-like and gaseous-like character, respectively, can occur.

For positive  $a_{sc}$ , the “standard” HF/GP treatment has been improved by including an additional mean-field term [2,35,36]. This modified treatment leads to an improved description of BECs with small and medium interaction parameters, however, exhibits divergences similar to that observed for the standard mean-field treatment as  $a_{sc} \rightarrow \infty$ . Therefore the modified mean-field treatment does not overcome the limitations of the standard mean-field treatment addressed above.

To improve upon the GP (or equivalently, the HF) treatment, several groups [37–44] developed mean-field formalisms within the shape-independent contact potential approximation. These approaches go beyond typically applied approximations by introducing a molecular field, and are aimed at describing condensate physics in the presence of a Feshbach resonance. Application of these formalisms to calculating the energetics as a function of  $a_{sc}$ , i.e., in the regions where  $a_{sc} \approx a_{cr}$  and  $|a_{sc}| \rightarrow \infty$  would be useful. The present study may then be used to benchmark such treatments, and would thus provide a strong link between many-body and mean-field treatments.

To make further contact with mean-field treatments, comparisons between our three-body excitation frequencies and those calculated within the random phase approximation can be made. This comparison will be discussed in a future publication.

## V. CONCLUSIONS

This paper discusses microscopic studies for three  $^{87}\text{Rb}$  atoms interacting via a sum of simple two-body model potentials under external confinement. Our study is important in light of recent experiments of atomic gases trapped in an optical lattice with an occupancy of 1-3 atoms per lattice site [6,7]. These experiments open the opportunity to systematically study strongly-interacting few-body systems, and therefore enter regimes discussed in the present paper from a theoretical microscopic point of view. The overall behavior of the zero temperature energy levels discussed in Secs. III and IV is independent of the exact shape of the two-body potential, though the detailed behavior of the energy levels and of the hyperradial potential curves at small hyperradii  $R$  depends on the shape of the two-body potential. The goal of this paper is to point out the gross behavior of the energy levels as a function of the two-body  $s$ -wave scattering length  $a_{sc}$ . Therefore, we consider only one class of two-body potentials. Our main results are derived for a relatively large trapping frequency,  $\nu_{ho} = 78\text{kHz}$ . As pointed out in Sec. III, dependencies on  $\nu_{ho}$  exist, however, the gross features of the energy level scheme are independent of the magnitude of  $\nu_{ho}$ .

Our time-independent calculations, performed mostly within the adiabatic approximation, include molecular-like and gaseous-like states, whereas standard mean-field treatments only treat the latter states. Our study reveals a microscopic understanding of the decay of a BEC in agreement with a study by Bohn *et al.* [33]. Furthermore, the present microscopic three-body study reveals a *smooth non-diverging* behavior of the energy levels around the pole region where  $|a_{sc}| \rightarrow \infty$ , and provides a detailed picture of the corresponding physics through analysis of hyperspherical potential curves.

Section IV compares our microscopic energy levels with those calculated at the HF level. While mean-field theories are commonly derived in the large particle limit, the HF equation is valid for any number of particles and density (though it might result in a more accurate description for systems with large  $N$  and low density). The energy level pattern for systems with more than three particles may differ in detail from our three-body energy levels presented here, however, the overall behavior will be similar and we expect our main conclusions to generalize to systems with more than  $N = 3$  particles.

Our study raises several discussion points. Most of all, we have only briefly discussed the effect of channel coupling on the behavior of the energy level scheme (see Fig. 5). To obtain detailed information about the dynamics of the condensate, inclusion of channel coupling, or at least a Landau-Zener-type analysis, is required. Such an analysis would allow the following question to be addressed (see Fig. 2): Is it possible to form a BEC with positive  $a_{sc}$  that resides in a hyperradial curve other than the lowest curve with BEC character, and then decrease  $a_{sc}$  until  $a_{sc} < a_{cr}$  (e.g. through the use of a Feshbach resonance) without destroying the condensate? Answers to this question certainly require a more detailed analysis, and will be left for future study.

To extend the present work to many (more than four) particles is computationally infeasible. We hope, however, that our results can eventually be compared with modified mean-field treatments that implicitly include molecular states [37–44]. Our study may then provide an additional link between many-body and mean-field physics. Lastly, our work relates to various many-body treatments using hyperspherical coordinates [33,34,45,46] that neglect molecular physics. (An exception is the recent study by Sørensen *et al.* [46], which includes molecular states explicitly.)

## ACKNOWLEDGMENTS

We thank B. D. Esry for providing access to his B-spline code, and J. Macek for suggesting that we apply Eqs. (4) and (5) of Reference [20]. This work was supported by the National Science Foundation.

- 
- [1] F. Dalfovo, S. Giorgini, L. P. Pitaevskii, and S. Stringari, *Rev. Mod. Phys.* **71**, 463 (1999).
  - [2] E. Braaten and A. Nieto, *Phys. Rev. B* **56**, 14745 (1997).
  - [3] E. H. Lieb, R. Seiringer, and J. Yngvason, *Phys. Rev. A* **61**, 043602 (2000).
  - [4] S. L. Cornish *et al.*, *Phys. Rev. Lett.* **85**, 1795 (2000).
  - [5] E. A. Donley *et al.*, *Nature* **412**, 295 (2001).
  - [6] M. Greiner *et al.*, *Nature* **415**, 39 (2002).
  - [7] H. T. C. Stoof, *Nature* **415**, 25 (2002).
  - [8] L. P. Pitaevskii, *J. Exptl. Theoret. Phys. (U.S.S.R.)* **40**, 646 (1961).
  - [9] E. P. Gross, *Nuovo Cimento* **20**, 454 (1961).

- [10] E. P. Gross, *J. Math. Phys.* **4**, 195 (1963).
- [11] B. D. Esry, *Phys. Rev. A* **55**, 1147 (1997).
- [12] S. A. Morgan, *J. Phys. B: At. Mol. Opt.* **33**, 3847 (2000).
- [13] M. J. Davis, S. A. Morgan, and K. Burnett, *Phys. Rev. Lett.* **87**, 160402 (2001).
- [14] Y. Kagan, A. E. Muryshev, and G. V. Shlyapnikov, *Phys. Rev. Lett.* **81**, 933 (1998).
- [15] R. A. Duine and H. T. C. Stoof, *Phys. Rev. Lett.* **86**, 2204 (2001).
- [16] H. Saito and M. Ueda, *Phys. Rev. Lett.* **86**, 1406 (2001).
- [17] B. D. Esry, C. H. Greene, and J. P. Burke Jr., *Phys. Rev. Lett.* **83**, 1751 (1999).
- [18] R. J. Dodd *et al.*, *Phys. Rev. A* **54**, 661 (1996).
- [19] B. D. Esry, C. H. Greene, Y. Zhou, and C. D. Lin, *J. Phys. B: At. Mol. Opt.* **29**, L51 (1996).
- [20] E. Nielsen and J. H. Macek, *Phys. Rev. Lett.* **83**, 1566 (1999).
- [21] P. F. Bedaque, E. Braaten, and H.-W. Hammer, *Phys. Rev. Lett.* **85**, 908 (2000).
- [22] O. I. Kartavtsev and J. H. Macek, accepted for publication (2002).
- [23] E. Braaten and H.-W. Hammer, *Phys. Rev. Lett.* **87**, 160407 (2001).
- [24] B. D. Esry and C. H. Greene, *Phys. Rev. A* **60**, 1451 (1999).
- [25] J. Macek, *J. Phys. B* **1**, 831 (1968).
- [26] C. D. Lin, *Phys. Rep.* **257**, 1 (1995).
- [27] Y. Zhou, C. D. Lin, and J. Shertzer, *J. Phys. B: At. Mol. Opt.* **26**, 3937 (1993).
- [28] R. C. Whitten and F. T. Smith, *J. Math. Phys.* **9**, 1103 (1968).
- [29] J. Avery, *Hyperspherical Harmonics: Applications in Quantum Theory* (Kluwer Academic Publishers, Dordrecht, Boston, London, 1989).
- [30] D. Blume, C. H. Greene, and B. D. Esry, *J. Chem. Phys.* **113**, 2145 (2000).
- [31] L. D. Landau and E. M. Lifshitz, *Quantum Mechanics (Non-relativistic theory), Vol. 3, 3rd Edition* (Butterworth Heinemann, Oxford, 1977).
- [32] D. Blume and C. H. Greene, accepted for publication in *Phys. Rev. A* (2002).
- [33] J. L. Bohn, B. D. Esry, and C. H. Greene, *Phys. Rev. A* **58**, 584 (1998).
- [34] H. W. van der Hart, *Phys. Rev. A* **62**, 013601 (2000).
- [35] A. Fabrocini and A. Polls, *Phys. Rev. A* **60**, 2319 (1999).
- [36] D. Blume and C. H. Greene, *Phys. Rev. A* **63**, 063601 (2001).
- [37] P. D. Drummond, K. V. Kheruntsyan, and H. He, *Phys. Rev. Lett.* **81**, 3055 (1998).
- [38] E. Timmermans, P. Tommasini, M. Hussein, and A. Kerman, *Phys. Rep.* **315**, 199 (1999).
- [39] E. Timmermans *et al.*, *Phys. Rev. Lett.* **83**, 2691 (1999).
- [40] M. Mackie, R. Kowalski, and J. Javanainen, *Phys. Rev. Lett.* **84**, 3803 (2000).
- [41] K. Góral, M. Gajda, and K. Rzążewski, *Phys. Rev. Lett.* **86**, 1397 (2001).
- [42] M. Holland, J. Park, and R. Walser, *Phys. Rev. Lett.* **86**, 1915 (2001).
- [43] M. Holland, S. J. J. M. F. Kokkelmans, M. L. Chiofalo, and R. Walser, *Phys. Rev. Lett.* **87**, 120406 (2001).
- [44] J. J. Hope and M. K. Olsen, *Phys. Rev. Lett.* **86**, 3220 (2001).
- [45] Y. E. Kim and A. L. Zubarev, *J. Phys. B* **33**, 3905 (2000).
- [46] O. Sørensen, D. V. Fedorov, A. S. Jensen, and E. Nielsen, cond-mat/0110069 v1 3 Oct 2001.

FIG. 1. Upper panel: Adiabatic potential curves,  $U_\nu$ , plus trapping potential,  $V_{trap}$  ( $\nu_{ho} = 78\text{kHz}$ ,  $a_{ho} = 731\text{a.u.}$ ), as a function of the hyperradius  $R$  for  $N_b = 2$  and  $a_{sc} = 228\text{a.u.}$ . The dashed curves ( $\nu = 0, 1$ ) describe molecular-like states while the solid curves describe gaseous-like states. Lower panel: Blowup of the gaseous region. In addition, dotted lines show the potential curves for vanishing interaction potential  $V$ . Note the logarithmic  $R$  scale.

FIG. 2. Internal energy levels  $E_{\nu n}^{int}$  (solid lines) as a function of  $[\arctan(a_{sc}/a_{ho})]/\pi$  for three particles in a spherical trap with trapping frequency  $\nu_{ho} = 78\text{kHz}$  ( $a_{ho} = 731\text{a.u.}$ ). Dotted lines indicate the “internal” HF energy  $E_{HF}^{int}$  (see text). The “first cycle” ( $N_b = 1$ , see text) corresponds to  $[\arctan(a_{sc}/a_{ho})]/\pi \in [-0.5, -1.5]$ , and the “second cycle” ( $N_b = 2$ , see text) to  $[\arctan(a_{sc}/a_{ho})]/\pi \in [-1.5, -2.5]$  ( $[\arctan(a_{sc}/a_{ho})]/\pi = -0.5, -1, -1.5, -2, -2.5$  corresponds to  $|a_{sc}| = \infty, 0, \infty, 0, \infty$ ). Labels A-F indicate systems with different scattering length for which Fig. 3 shows the corresponding adiabatic potential curves (A:  $a_{sc} = 2138\text{a.u.}$ ; B:  $a_{sc} = 103\text{a.u.}$ ; C:  $a_{sc} = 0\text{a.u.}$ ; D:  $a_{sc} = -31\text{a.u.}$ ; E:  $a_{sc} = -130\text{a.u.}$ ; and F:  $a_{sc} = -1970\text{a.u.}$ ).



FIG. 3. Adiabatic potential curves,  $U_\nu$ , plus trapping potential,  $V_{trap}$ , for three particles in a trap with  $\nu_{ho} = 78\text{kHz}$  ( $a_{ho} = 731\text{a.u.}$ ) as a function of the hyperradius  $R$ . Solid lines indicate the numerical potential curves for A:  $a_{sc} = 2138\text{a.u.}$ ; B:  $a_{sc} = 103\text{a.u.}$  ( $d$ -wave shape resonance); C:  $a_{sc} = 0\text{a.u.}$ ; D:  $a_{sc} = -31\text{a.u.}$  (first signature of decay); E:  $a_{sc} = -130\text{a.u.}$  (vanishing potential barrier); and F:  $a_{sc} = -1970\text{a.u.}$ . These scattering lengths are also indicated in Fig. 2. The thick solid line indicates the lowest gaseous level (panel A-D), and the “decayed” condensate state (panel E and F), respectively. In addition, dotted lines show the potential curves for vanishing two-body interaction potential.

FIG. 4. Internal energy levels  $E_{\nu n}^{int}$  (solid lines) as a function of  $[\arctan(a_{sc}/a_{ho})]/\pi$  for three particles in a spherical trap with trapping frequency  $\nu_{ho} = 780\text{Hz}$  ( $a_{ho} = 7307\text{a.u.}$ ) for  $N_b = 2$ . Diamonds indicate the internal energies at large negative  $a_{sc}$ . A dotted line indicates the “internal” HF energy  $E_{HF}^{int}$  (see text).

FIG. 5. Internal adiabatic energy levels  $E_{\nu n}^{int}$  (dotted, solid and dashed lines) together with energies calculated using the coupled-adiabatic-channel approach including four channels (pluses) as a function of  $[\arctan(a_{sc}/a_{ho})]/\pi$  for three particles in a spherical trap with trapping frequency  $\nu_{ho} = 78\text{kHz}$  ( $a_{ho} = 731\text{a.u.}$ ). Dotted lines indicate “plunging” molecular levels, while solid and dashed lines indicate energy levels in the lowest and in the second lowest gaseous adiabatic potential curve, respectively.

Fig. 1

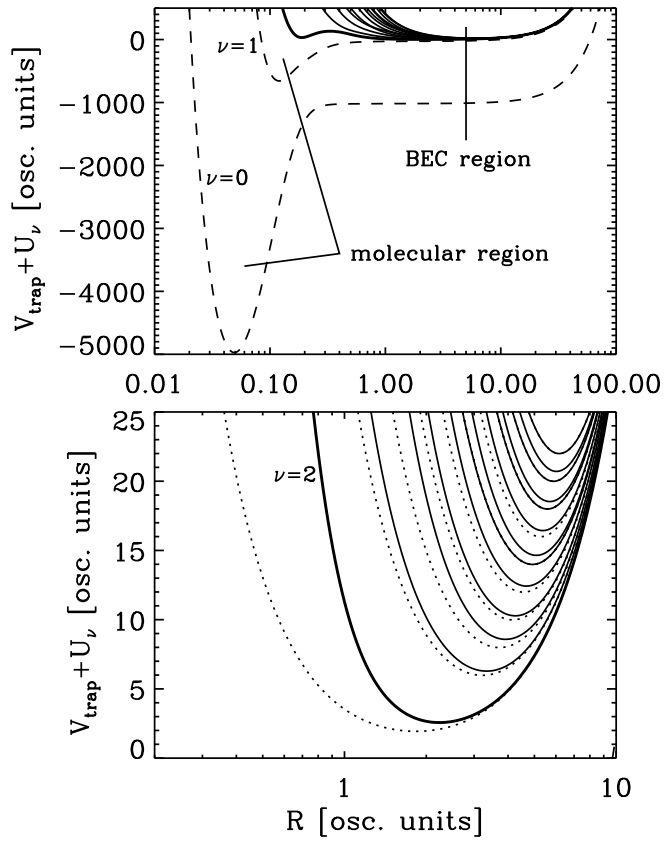


Fig. 2

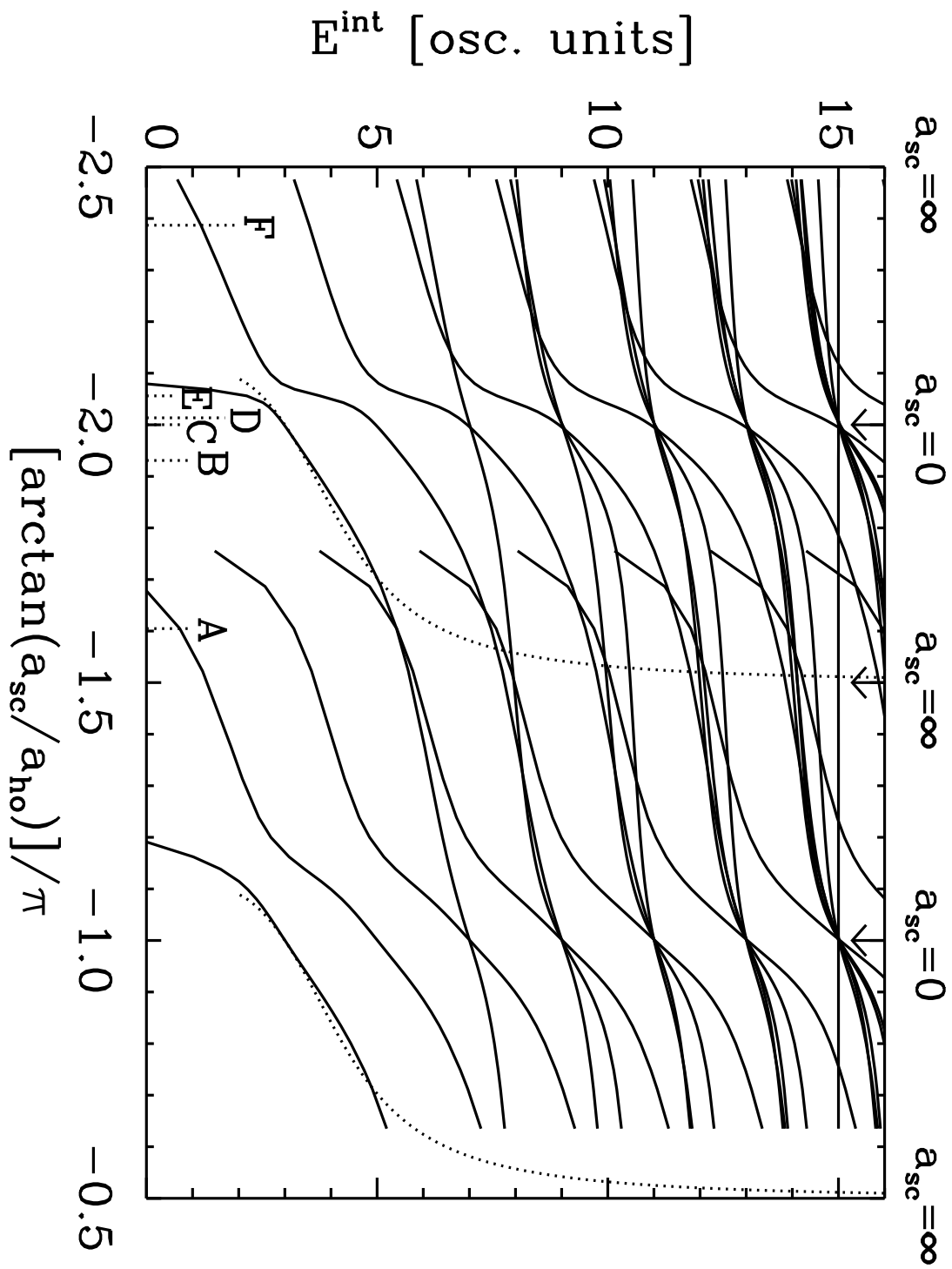


Fig. 3

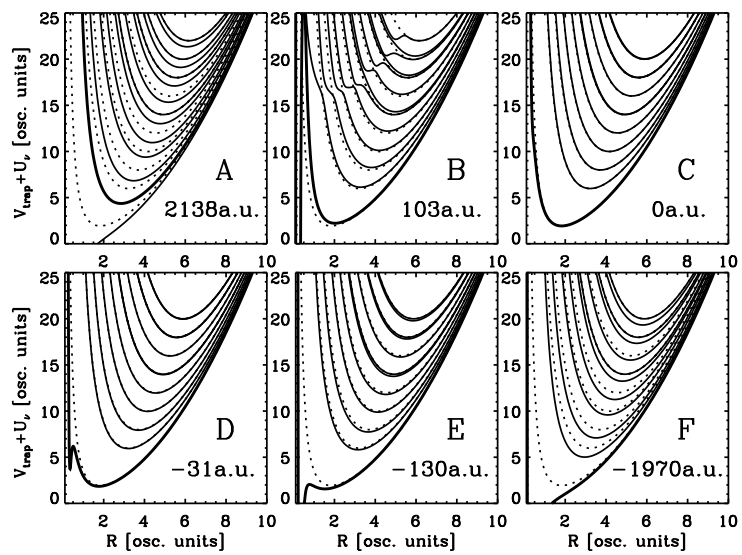


Fig. 4

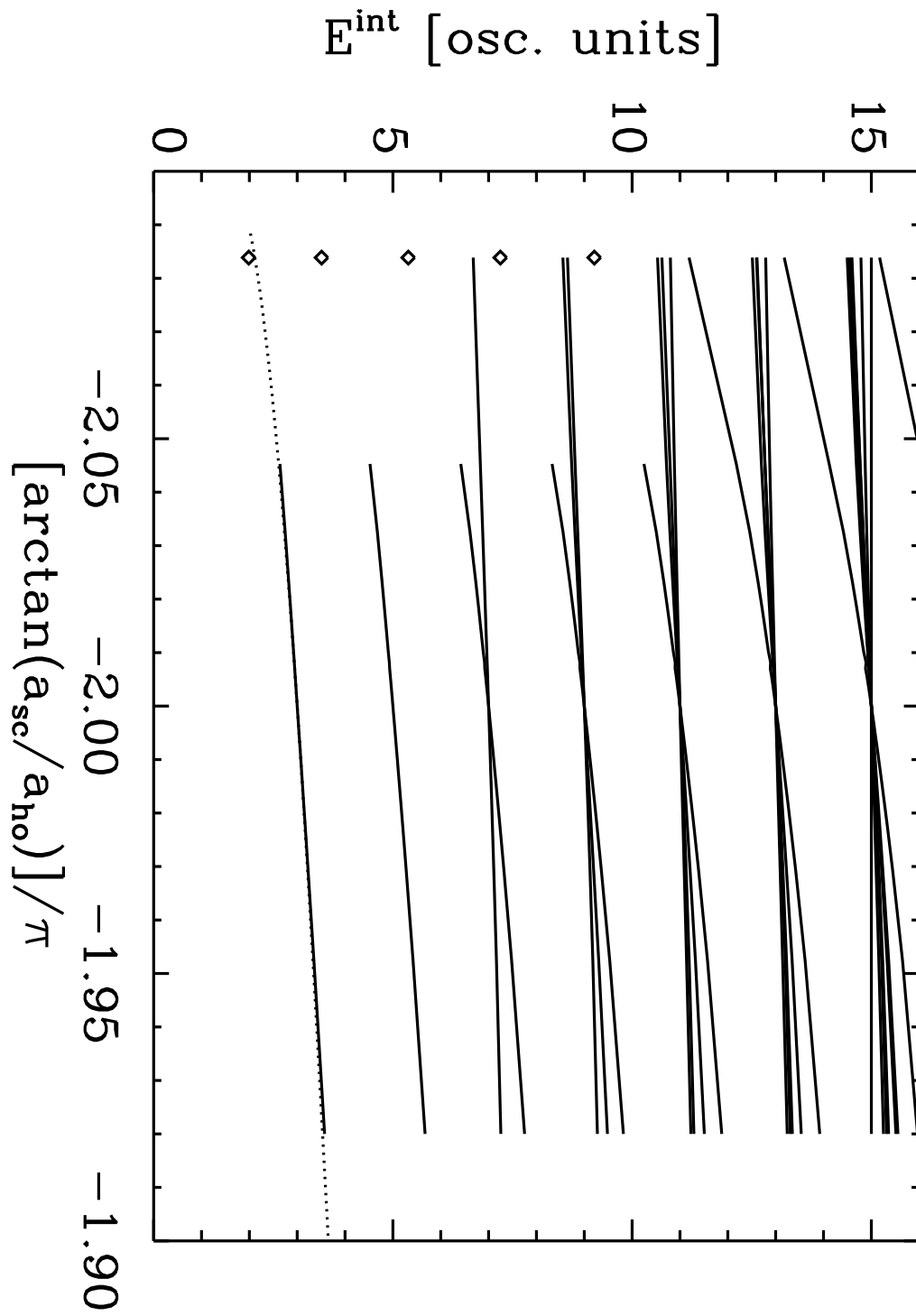


Fig. 5

